Supporting Information for

Low-voltage-hysteresis aluminum-sulfur battery with covalently functionalized mesoporous graphene

Weiqin Chu, [a,b#] Shiman He,[c #] Shiqi Liu [a,b], Xu Zhang,[a,b*] Shuaixia Li [a,b] and Haijun Yu [a,b*]

[a.] Institute of Advanced Battery Materials and Devices, Faculty of Materials and Manufacturing, Beijing University of Technology, Beijing, 100124, P. R. China

[b.] Key Laboratory of Advanced Functional Materials, Ministry of Education, Beijing University of Technology, Beijing, 100124, P. R. China.

[c.] Guangdong Provincial Key Laboratory of Advanced Energy Storage Materials, School of Materials Science and Engineering, South China University of Technology, Guangzhou, 510640, China.

*Correspondence: hj-yu@bjut.edu.cn; zhangx@bjut.edu.cn

[#] These authors contributed equally to this work.

Experimental method

Material fabrication

Mesoporous graphene (MPG) was synthesized by chemical vapor deposition (CVD) using CH_4 as the carbon source and $Mg(OH)_2$ as the template.[1] Pyridyl-modified mesoporous graphene (Py-MPG) was prepared by the covalent functionalization of MPG using a sodide reduction method.[2] A reductive solution of $[K(15\text{-crown-}5)_2]Na$ was prepared by adding fresh NaK and 15-crown-5 (Aldrich, 98%)with a molar ratio of 1:2 in THF inside an argon glovebox at room temperature. MPG was then added into the solution and stirred for 30 min for the efficient reduction. A solution of 4-iodopyridine as the electrophilic addition reagent in THF was then slowly added into the suspension and stirred for 30 min. The suspension was filtered and subsequently washed by diluted HCl, ethanol, and THF to yield Py-MPG. Mesoporous CMK-3 (XF NANO, Nanjing) was used as received.

For the preparation of sulfur composite cathode materials, elemental sulfur and carbon materials were first milled in a weight ratio of 3:7 for 30 min. The milled mixture was then heated inside a hydrothermal reactor under argon at 155 °C for 12 h.[3]

Battery assembly

The cathodes of Al-S batteries were prepared by combining 70 wt.% sulfur composite cathode material (S@CMK-3, S@MPG, and S@Py-MPG), 10 wt.% PTFE binder, and 20 wt.% super P. Al-S batteries were assembled by using the S cathodes, Al foil (99.9%, 0.05 mm, Beijing Trillion Metals Co., Ltd) as the anode, ~100 μL $AlCl_3$/Acetamide ($AlCl_3$/AcA, 1.3/1) as the electrolyte, and Whatman Glass fiber as the separator, in a Swagelok configuration.

Electrochemical analysis and characterizations

Al-S batteries were tested using Land instrument (Wuhan LAND electronics Co., Ltd.) at 25 °C. Cyclic voltammogram (CV) was performed using a Solartron electrochemical

workstation. The galvanostatic intermittent titration technique (GITT) were performed at a current density of 100 mA g^{-1} for 1 h between 0.1-1.7 V, followed by a relaxation step for 2 h.

The morphologies of materials were examined by scanning electron microscopy (SEM, FEI VERIOS 460) and transmission electron microscopy (TEM, JEOL JEM-2100 microscope) at an accelerating voltage of 200 kV. The specific surface areas were calculated based on the multi-point Brunauer-Emmett-Teller (BET) method. Pore size distribution (PSD) curves were computed based on the density functional theory (DFT) method. The samples were first degassed at temperatures <300 °C. X-ray photoelectron spectroscopy (XPS) measurements were performed on a Thermo Scientific ESCALAB 250 Xi system, which was equipped with an Al Ka source (1486.6 eV) with a base pressure below 10^{-10} mbar. Raman spectra were recorded on a confocal micro-Raman spectrometer (WITec alpha300) using a 532 nm laser. N_2 adsorption/desorption analysis was conducted using an Automatic physical adsorption analyzer (ASAP 2020HD88). Thermal Gravimetric Analysis (TGA) analysis of S composite cathode materials were performed on a NETZSCH STA 449F5 Libra in Ar atmosphere, ranging from room temperature to 600 °C (10 °C min^{-1}).

Additional figures and tables

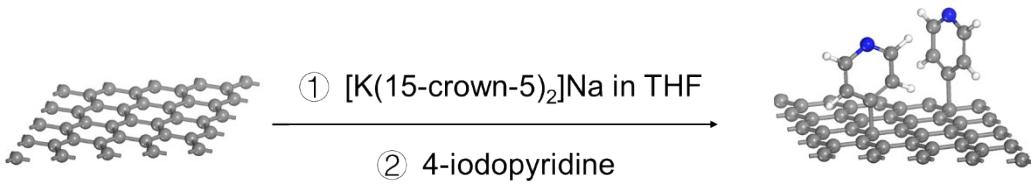

Fig. S1 Schematic illustration of the functionalization of MPG using a sodide reduction method with 4-iodopyridine as the electrophilic addition reagent.

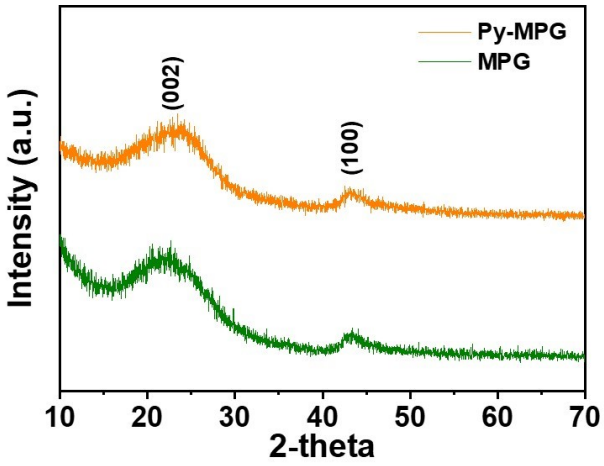

Fig. S2 XRD patterns of MPG (a) and Py-MPG (b).

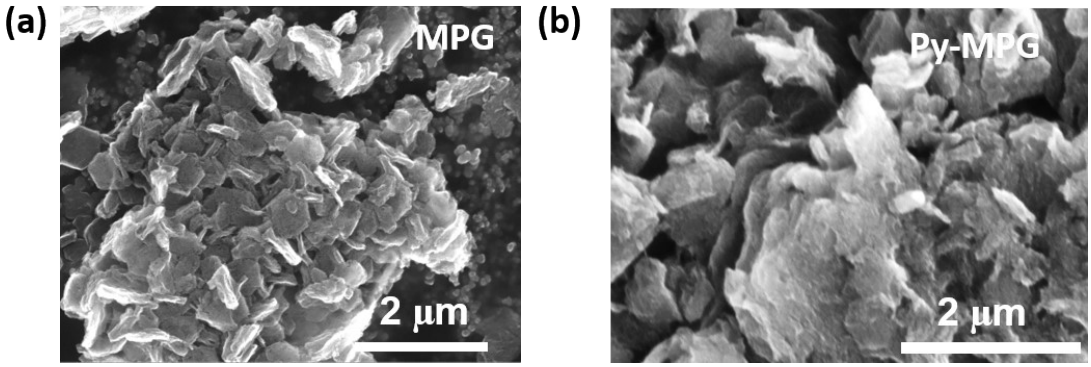

Fig. S3 SEM images of MPG (a) and Py-MPG (b).

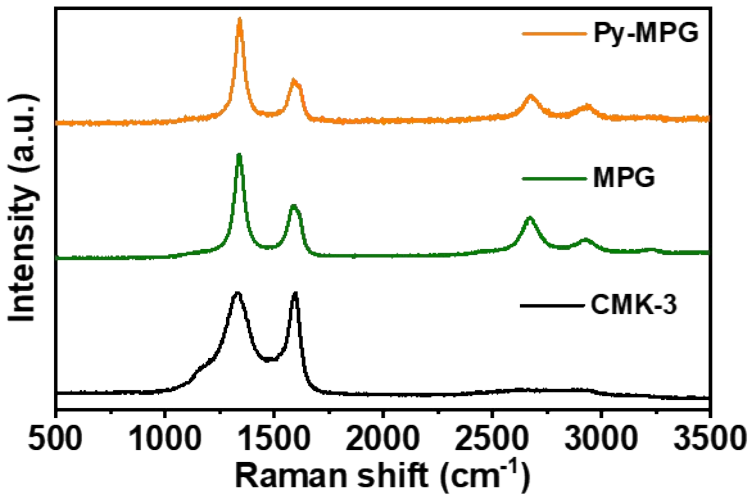

Fig. S4 Raman spectra of CMK-3, MPG and Py-MPG.

The Raman 2D peak (~2680 cm^{-1}) of carbon materials can represent the degree of graphitic structure. As shown in Fig. S4, both MPG and Py-MPG show noticeable 2D bands, implying the high degrees of graphitic structures. On the other hand, the Raman D peak can reflect the defect degree. When the defect density of a carbon material is relatively high, the full width at half maxima ($FWHM_D$) of the D peak is important to compare the defect degree.[4, 5] As shown in Table S1, CMK-3 has much larger $FWHM_D$ than MPG and Py-MPG, demonstrating its high defect density compared with MPG and Py-MPG.

Table S1 Typical parameters of Raman spectra of Py-MPG, MPG and CMK-3.

	Py-MPG	MPG	CMK-3
I_{2D}/I_G	0.61	0.77	0.05
I_D/I_G	2.54	2.01	0.98
$FWHM_D$	45	40	143

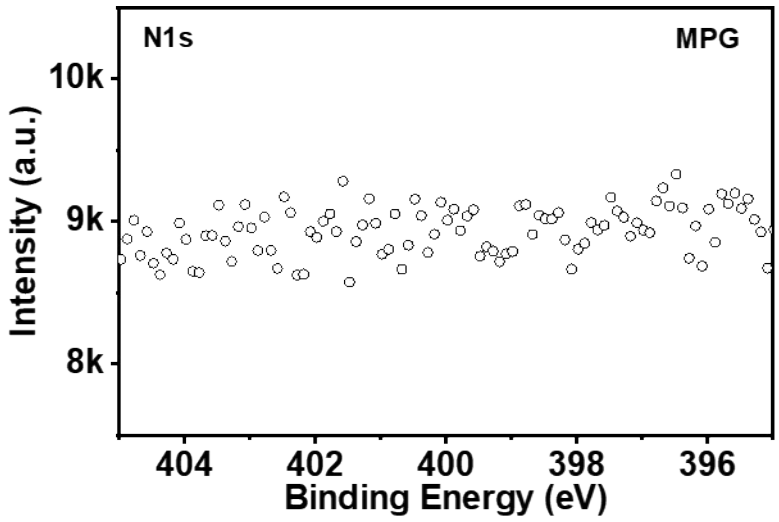

Fig. S5 XPS N1s spectrum of MPG.

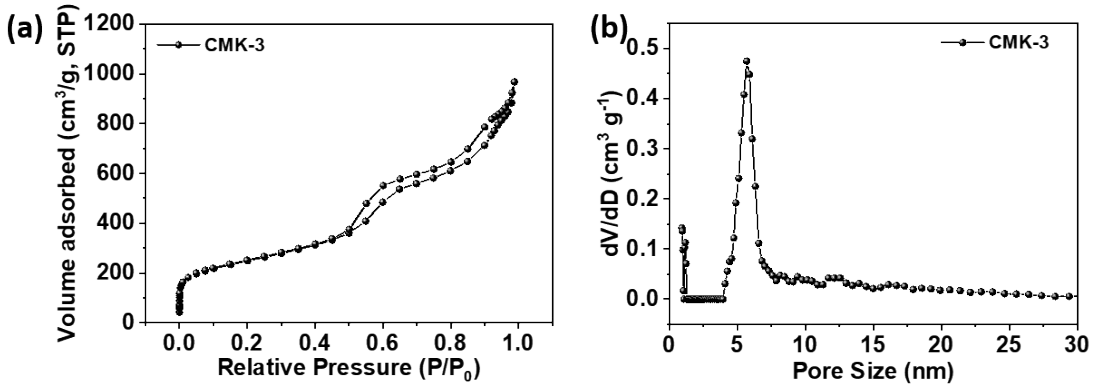

Fig. S6 Nitrogen adsorption–desorption isotherm profile (a) and pore size distribution (b) of CMK-3.

The nitrogen adsorption-desorption isotherm profile in Fig.S8 shows the surface area of CMK-3 is 876 m^2 g^{-1}, and the pore-size distribution is about 4~7.5 nm.

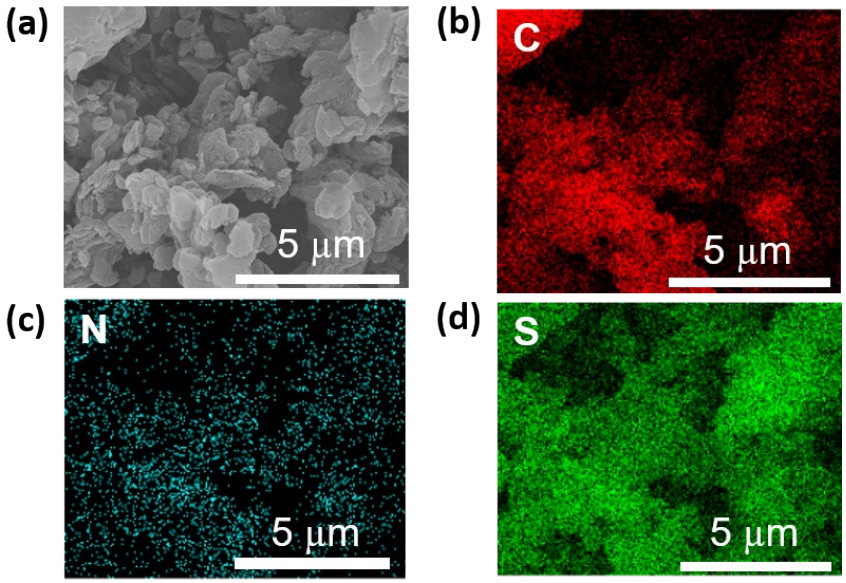

Fig. S7 Energy dispersive spectroscopy (EDS) maps of C, N, and S in S@Py-MPG.

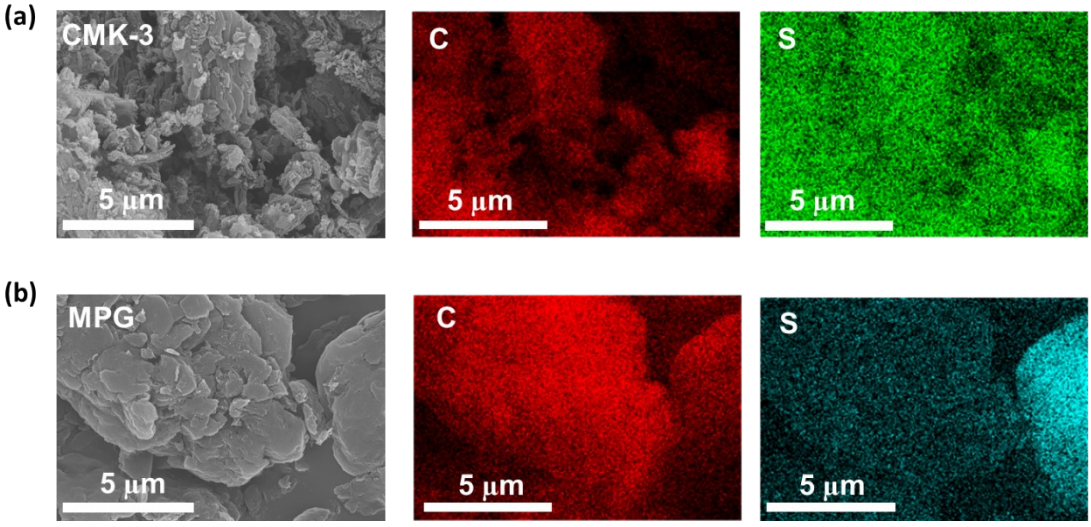

Fig. S8 EDS maps of C and S in S@CMK-3 (a) and S@MPG (b).

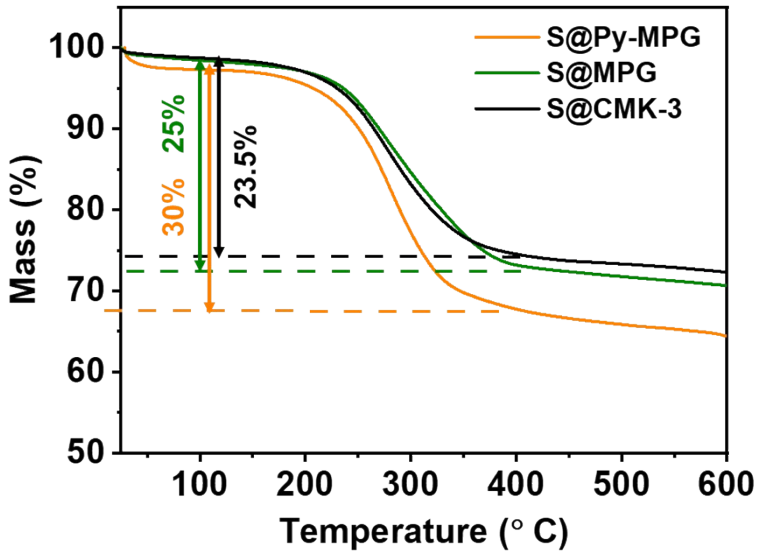

Fig. S9 TGA profiles of S@Py-MPG, S@MPG, and S@CMK-3 in Ar atmosphere.

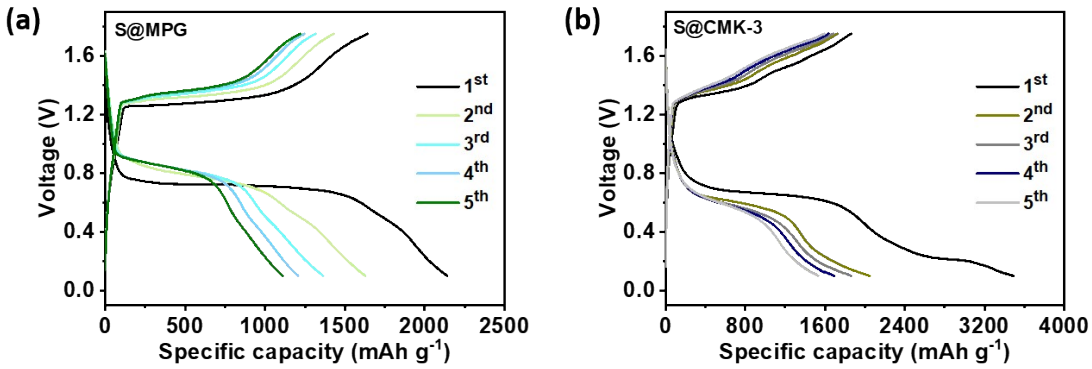

Fig. S10 The initial five charge/discharge profiles of the Al-S batteries using S@MPG (a) and S@CMK-3 (b) at 100 mA g^{-1}.

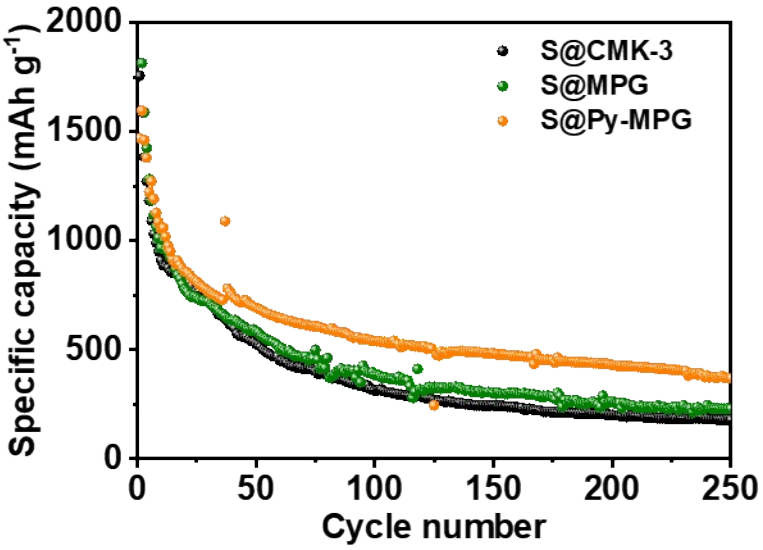

Fig. S11 Long-cycle performance of Al-S batteries using S@CMK-3, S@MPG and S@Py-MPG at 100 mA g^{-1}.

The Al-S battery using S@Py-MPG as the cathode material can stably operate for 250 cycles, with a final capacity of 370 mAh g^{-1}, significantly higher than those using S@MPG and S@CMK-3.

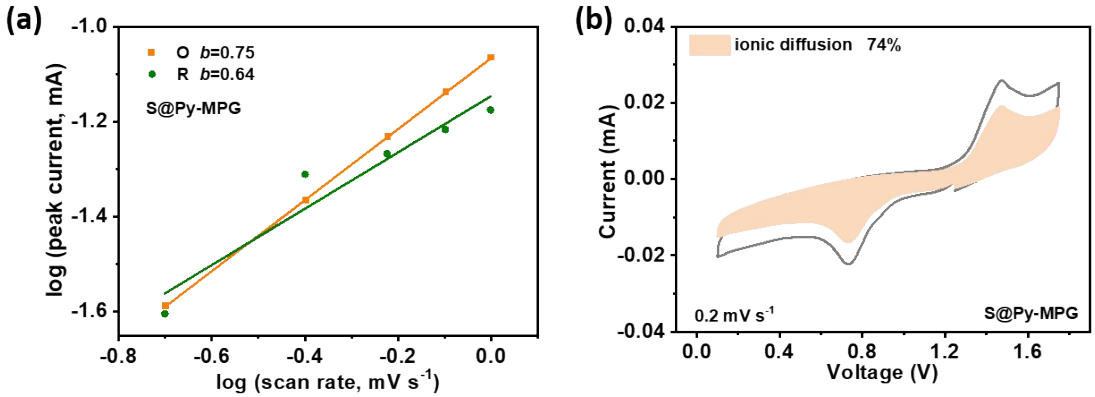

Fig. S12 (a) The corresponding plots of log (peak current, *i*) vs. log (scan rate, *v*) and the slop *b* of the redox peaks with CV curves at scanning rates of 0.2, 0.4, 0.6, 0.8, and 1.0 mV s^{-1} of the S@Py-MPG cathode (Fig. 3a). (b) The CV profile with the ionic diffusion contribution of the S@Py-MPG cathode at a scan rate of 0.2 mV s^{-1}.

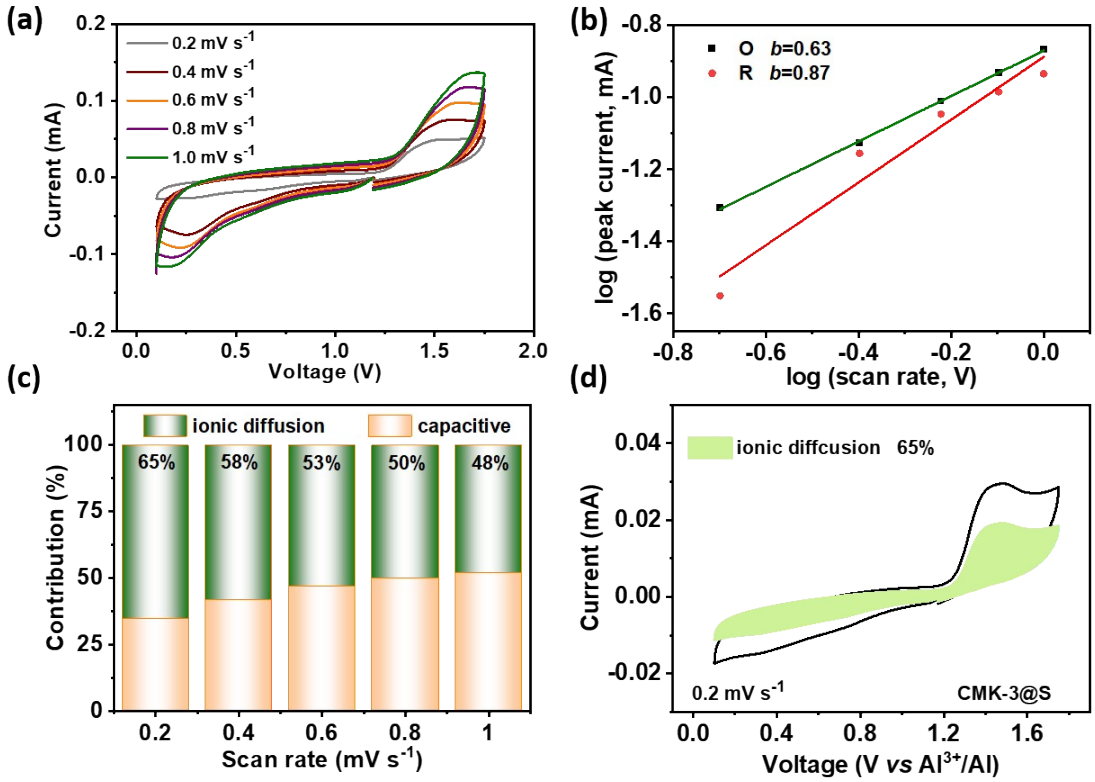

Fig. S13 Electrochemical kinetic analysis of the S@CMK-3 cathode. (a) CV curves at scan rates of 0.2, 0.4, 0.6, 0.8, 1.0 mV s^{-1}. (b) The corresponding plots of log (peak current, *i*) vs. log (scan rate, *v*) and the slop *b* of the redox peaks. (c) The ionic diffusion and capacitive contributions in S@CMK-3 at different scan rates. (d) The CV profile with the ionic diffusion contribution of S@CMK-3 electrodes at a scan rate of 1.0 mV s^{-1}.

The consecutive CV curves of the S@CMK-3-based Al-S battery was measured under incremental scan rates from 0.2 to 1.0 mV s^{-1}. A pair of redox peaks corresponding to oxidation (1.3-1.7 V) and reduction (0.2-0.3 V) of sulfur are clearly identified. Meanwhile, the peak currents and electrochemical polarization increase with the increase of scan rate. The *b* values are 0.63 and 0.87 for the oxidation and reduction peaks in Figs. 12b, which mean the energy storage mode of this electrode material is codetermined by ion diffusion and surface capacitance.[6] The percentage of ionic diffusion contribution (from 65% to 48%) decreased with the scan rate increased (0.2 mV s^{-1} to 1.0 mV s^{-1}), and the ionic diffusion contribution was 65% at 0.2 mV s^{-1} of S@CMK-3 cathode.

Table S2. The discharge/charge voltage plateau and voltage hysteresis of reported Al-S batteries and the S@Py-MPG-based Al-S battery.

Positive electrode materials	Discharge voltage plateau	Charge voltage plateau	Voltage hysteresis	Ref.
S@ Mesoporous carbon (CMK-3)	0.5 V	1.25 V	0.75 V	5
S@Co/C	0.6 V	1.4 V	0.8 V	6
S@ Carbon nanofiber (CNF)	0.76 V	1.50 V	0.74 V	7
S@ CoNG/C	0.75 V	1.51 V	0.76 V	8
S@CoNG	0.9 V	1.33 V	0.43 V	9
S@ CNF	0.95 V	1.75 V	0.8 V	21
S@Activated carbon cloth (ACC)	0.65 V	1.40 V	0.75 V	22
S@ Carbonized HKUST-1 matrix (HKUST-1-C)	0.4 V	1.55 V	1.15 V	23
S@ C	0.55 V	1.5 V	0.95 V	24
Sulfur/ Graphene/CoS_2	0.3 V	1.5 V	1.2 V	25
S@ Multiwalled carbon nanotubes (CNTs)	0.3 V	1.6 V	1.3 V	26
S@ Hollow carbon nanospheres (HC)	0.3 V	1.25 V	0.95 V	27
S/BN/ C	1.15 V	2.2 V	1.05 V	28
S@ TiN@N-doped-graphene	0.8 V	1.5 V	0.7 V	29
S@ Py-MPG	0.87 V	1.3V	0.43 V	Our work

Additional references

1. G. Ning, Z. Fan, G. Wang, J. Gao, W. Qian and F. Wei, *Chem. Commun.*, 2011, **47**, 5976-5978.
2. M. Biswal, X. Zhang, D. Schilter, T. K. Lee, D. Y. Hwang, M. Saxena, S. H. Lee, S. Chen, S. K. Kwak, C. W. Bielawski, W. S. Bacsa and R. S. Ruoff, *J. Am. Chem. Soc.*, 2017, **139**, 4202-4210.

3. W. Chu, X. Zhang, J. Wang, S. Zhao, S. Liu and H. Yu, *Energy Storage Mater.*, 2019, **22**, 418-423.
4. M. M. Lucchese, F. Stavale, E. H. M. Ferreira, C. Vilani, M. V. O. Moutinho, R. B. Capaz, C. A. Achete and A. Jorio, *Carbon*, 2010, **48**, 1592-1597.
5. L. G. Cancado, A. Jorio, E. H. Ferreira, F. Stavale, C. A. Achete, R. B. Capaz, M. V. Moutinho, A. Lombardo, T. S. Kulmala and A. C. Ferrari, *Nano Lett*, 2011, **11**, 3190-3196.
6. X. Peng, Y. Xie, A. Baktash, J. Tang, T. Lin, X. Huang, Y. Hu, Z. Jia, D. J. Searles, Y. Yamauchi, L. Wang and B. Luo, *Angew. Chem. Int. Ed. Engl.*, 2022, **61**, e202203646.